Modeling the Effects of Bed Topography on Fluvial Erosion by Saltating Bed Load

by

Shahen Ahmed Huda

B.A., Dartmouth College, 2010

B.E., Thayer School of Engineering, Dartmouth College, 2011

A thesis submitted to the

Faculty of the Graduate School of the

University of Colorado in partial fulfillment

of the requirements for the degree of

Master of Science

Department of Geological Sciences

2013

This thesis entitled:
Modeling the Effects of Bed Topography on Fluvial Erosion by Saltating Bed Load
written by Shahen Ahmed Huda
has been approved for the Department of Geological Sciences

Eric Small Tilton

Prof. Robert S. Anderson

Assoc. Prof. Gregory E. Tucker

Date ____________

The final copy of this thesis has been examined by the signatories, and we find that both the content and the form meet acceptable presentation standards of scholarly work in the above mentioned discipline.

Huda, Shahen Ahmed (M.S., Geological Sciences)

Modeling the Effects of Bed Topography on Fluvial Erosion by Saltating Bed Load

Thesis directed by Prof. Eric Small Tilton

Abrasion by bed load is a dominant erosional mechanism of fluvial incision into bedrock. The foremost saltation-abrasion model states that erosion rate is linearly dependent on the flux of impact kinetic energy in the vertical direction and on the fraction of the bed that is not covered by alluvium [*Sklar and Dietrich*, 2004]. Results from this model show that erosion is greatest in moderate flows with medium-sized grains. However, the saltation-abrasion model is only applicable to smooth, flat beds, which almost never appear in nature. Despite the fact that the floors of most bedrock channels are sloped and sculpted into rough topography, this model has been applied in numerous studies to model evolution of streams and landscapes. Here, the saltation-abrasion model is modified for bed load transport over simple bed topography by accounting for kinetic energy flux normal to topography. Averaged over the entire domain, erosion rates can increase by orders of magnitude depending on grain size and flow strength. This erosion is focused on flow-facing slopes, and is corroborated by experimental and field observations. The amount of erosion enhancement is greater for smaller grains and stronger flows, even if the topography is small and low-angle. This is in direct opposition to the findings of *Sklar and Dietrich* [2004]. Therefore, bed topography should be considered when attempting to estimate erosion rates in bedrock channels.

Acknowledgements

This research is supported by a grant from the National Science Foundation Geomorphology and Land Use Dynamics panel (EAR 0922235).

This thesis would be impossible if not for my advisor, Eric Small Tilton, for his patience, encouragement, and guidance through my time at CU.

I also thank my fellow graduate students for their support intellectually and emotionally. In particular I thank Sarah Evans, Nadine Reitman, Cailey Condit, Jonathan Galeano, and Peter Shellito for listening to my complaints and problems, sending me funny emails, keeping my spirits up as I stared at a computer screen for hours on end, and generally being great friends.

Joy Campbell has been the source of continued laughs, conversations, unwavering encouragement, support and friendship, and without her this would have been much more difficult.

Finally, I offer special thanks to my parents for the curiosity and enthusiasm for learning they passed down to me, as well as the encouragement, love, and support they have always offered.

Contents

Chapter

Tables

Table

Figures

Figure

Chapter 1

Introduction

Erosion of bedrock-floored channels is a critical process in driving landscape evolution [e.g. *Howard et al.*, 1994]. However, surprisingly little is known about the physical controls on erosion of bedrock stream beds [*Whipple et al.*, 2000]. Most models of landscape evolution assume bedrock incision is proportional to flow intensity, combining the effects of rock strength, channel slope, discharge, sediment supply, and sediment characteristics into several parameters not tied to any distinct mechanism [e.g. *Anderson*, 1994; *Tucker and Slingerland*, 1994].

Streams incise into bedrock by several mechanisms, including cavitation [e.g. *Barnes*, 1956; *Allen*, 1971; *Wohl and Ikeda*, 1998], dissolution [e.g. *Allen*, 1971; *Richardson and Carling*, 2005], abrasion by bed load and suspended load [e.g. *Whipple et al.*, 2000; *Sklar and Dietrich*, 2001; *Wilson et al.*, 2013], and plucking of rock fragments by fluid shear stresses [e.g. *Allen*, 1971; *Whipple et al.*, 2000]. Since all rivers transport sediment in some quantity, the most ubiquitous erosive processes are via abrasion; other processes require certain flow and/or substrate conditions.

Saltation is the subject of numerous studies. *Einstein* [1950] found bed load thickness to be about twice particle size, and saltation length to be a function of particle size, shape, and hydraulic characteristics. Several studies have investigated saltation in water using high-speed photography and videography to determine saltation height, length, and particle velocity [e.g. *Abbott and Francis*, 1977; *Sekine and Kikkawa*, 1992; *Hu and Hui*, 1996a,b].

Other studies have simulated salatation trajectories in air [e.g. *Anderson and Haff*, 1988; *Nasrollahi et al.*, 2008] and in water [e.g. *Wiberg and Smith*, 1985; *Lee and Hsu*, 1994]. Particles in these simulations are subject to inertia force, submerged weight, lift force, and drag force. In addition to lift due to shear, the Magnus effect creates a lift force due to particle spin [*Rubinow and Keller*, 1961]. Trajectories can be calculated by determining force balances on a particle as it moves in time and space.

Abrasion by bed load is the focus of this study for several reasons. As all rivers transport sediment, erosion by abrasion is ubiquitous, and by definition bed load interacts with the bed far more than suspended load. Particle impacts with the bed are an efficient mechanism for the transfer of energy from the flow to the bed. Additionally, much is known about the motion of saltating bed load, as described above, and it has been shown that saltating grains can produce measurable wear [*Sklar and Dietrich*, 2001]. Finally, other mechanisms of erosion occur under limited conditions; an analysis of bed load abrasion is applicable to all streams.

Sklar and Dietrich [2004] present a physically based model for bedrock incision due to abrasion from saltating bed load using average saltation characteristics taken from several studies. Simply put, this model states that erosion rate due to saltating bed load is a function of average volume eroded per saltation impact, impact rate, and bedrock exposure. Characteristics of both the impacting grain as well as the bedrock substrate affect the erosive potential of saltating material. Most important to this study, volume eroded is dependent on the vertical component of particle velocity as it impacts the bed. *Sklar and Dietrich* [2004] predict maximum erosion at moderate sediment supplies due to tradeoffs between the so-called cover and tools effects and at moderate flow strengths due to tradeoffs between impact energy and frequency. This outcome of their model is not expected.

Erosion occurs due to the transfer of kinetic energy from the impacting particle to the bed, forcing a dislodging of volume related to the bed's tensile strength and elasticity. *Sklar* *and Dietrich* [2004] assume that only kinetic energy associated with the impacting particle's vertical velocity is transferred to the bed, implying that their model is applicable strictly to flat, horizontal beds. However, the majority of erosion due to abrasion occurs where the bed is topographically irregular [*Whipple et al.*, 2000].

Johnson and Whipple [2010] address the obvious shortcoming of characterizing saltation impacts solely by vertical velocity. Their flume experiments clearly show that erosion is focused on flow-facing slopes. In light of this, they propose modification to the *Sklar and Dietrich* [2004] model. Over topography, they speculate that the characteristic velocity transferring energy to the bed may be the horizontal particle velocity rather than the settling velocity. Furthermore, they suggest that with increased roughness, the impact rate will no longer scale with saltation length but with a characteristic roughness length, which will lead to a greater dependence of erosion rates on flow strength. The present study attempts to address this shortcoming by quantifying the energy transferred to the bed with a combination of vertical and horizontal particle velocities.

In a theoretical exercise, *Chatanantavet and Parker* [2009] modify *Sklar and Dietrich*'s [2004] model to include a single abrasion capability coefficient, which they claim can be generalized to include nonuniform bed topographies. However, they do not provide any examples to demonstrate the effectiveness of this coefficient. Furthermore, in their adaptation, *Chatanantavet and Parker* [2009] still calculate erosion rates with vertical impact velocity, not a normal velocity.

Smooth, flat beds rarely exist in nature. Both *Sklar* [2003] and *Whipple* [2004] note this limitation of the saltation-abrasion model. Instead, bedrock channel beds are typically sculpted into rounded topography [*Richardson and Carling*, 2005]. Both *Montgomery and Buffington* [1997] and *Wohl and Merritt* [2001] present classification schemes that define categories of bed morphology, which emphasize that streambeds are usually marked by potholes, flutes, knickpoints, and longitudinal grooves. Erosion is often focused on these features [*Whipple et al.*, 2000; *Johnson and Whipple*, 2010; *Wilson et al.*, 2013]. Mechanistic description of incision by abrasion cannot be divorced from the irregular geometry of the riverbed [*Wohl*, 1993; *Wohl and Ikeda*, 1997; *Whipple et al.*, 2000]. Despite this, many studies that investigate fluvial erosion into bedrock channels do not address the role of bedrock topography in determining erosion rates [e.g. *Howard et al.*, 1994; *Stock and Montgomery*, 1999; *Whipple and Tucker*, 1999, 2002].

Here, the model presented by *Sklar and Dietrich* [2004] is modified for application to a stream bed with simple topography. Using the approach presented by *Lamb et al.* [2008], turbulence is invoked to incorporate variability in individual saltation hops. A description of how the saltation-abrasion model is modified and applied is presented in Chapter 2. Erosion rates over topography are compared to erosion rates over a flat horizontal bed. The results include the effects of flow strength and grain size. Specifically, *Sklar and Dietrich*'s [2004] hypothesis of maximum erosion occurring at moderate flows with medium-sized grains is tested.

The modified saltation-abrasion model presented here does not account for the effects of topography on the overlying flow, so it is applicable only in scenarios where bed topography is small compared to flow depth. This is analyzed further in Chapter 4. Also analyzed in Chapter 4 is the use of regression statistics to simulate saltation trajectories, the implications of the assigned velocity profiles in the absence of complete data sets, and the implications of defining the distribution of alluvial cover with a single parameter. Finally, the results of the modified saltation-abrasion model presented here are compared to experimental and field observations from the literature.

Chapter 2

Model Development

2.1 Existing Model

The model presented here incorporates most of the assumptions made by *Sklar and Dietrich* [2004]. Analysis is limited to abrasion of rock by bed load, neglecting all other mechanisms for stream incision. Rolling and sliding grains are assumed to cause negligible wear; saltating grains are solely responsible for abrasion by bed load. For simplicity, all bed load is assumed to be composed of spherical grains of uniform size.

The model assumes uniform streamflow through the domain. Cross channel variations in shear stress, local variation in rock strength, and other reach-scale spatial heterogeneities are not accounted for, even though these factors may influence rate of incision by bed load abrasion [*Wobus et al.*, 2006; *Hancock et al.*, 2011].

Sklar and Dietrich's [2004] model of erosion by abrasion of a flat bed by saltating sediment grains can be stated as

$$E = V_i I_r F_e \tag{2.1}$$

where E is incision rate, V_i is the volume eroded per impact, I_r is impact rate per unit area, and F_e is the fraction of the streambed that is exposed to streamflow (See Appendix A for a list of symbols). The elements of the *Sklar and Dietrich* [2004] model are described below and form the basis of the model presented here.

2.1.1 Volume Eroded per Impact (V_i)

Erosion of brittle materials by low-velocity particle impacts occurs through the formation, growth, and intersection of a network of cracks [*Finnie*, 1960]. Though the erosion due to any single impact will depend on the local fracture density, the average wear rate scales with the flux of kinetic energy transferred by the impacting grains [*Engel*, 1976]. Invoking the class impact wear model of *Bitter* [1963], the volume eroded per impact (V_i) can be written

$$V_i = \frac{K_p - \epsilon_t}{\epsilon_v} \tag{2.2}$$

where ϵ_v is the total energy required to erode a unit volume of rock, ϵ_t is the threshold energy required for detachment, and K_p is the kinetic energy transferred to bedrock. Since the magnitude of the peak tensile stress varies with the normal component of impact velocity (v_n) [*Engel*, 1976], this velocity is used to determine K_p.

The resistance of rock to abrasion (parameterized in Eq. 2.2 by ϵ_v) depends on the capacity of the material to store energy elastically [*Engel*, 1976]. The capacity to store energy elastically (β) is defined as the area under the stress-strain curve at the yield stress, so

$$\epsilon_v = k_v \beta = k_v \frac{\sigma_T^2}{2Y} \tag{2.3}$$

where σ_T is the rock tensile yield stress, Y is Young's modulus of elasticity, and k_v is a dimensionless coefficient. Since variation in the modulus of elasticity of rocks is small, Y is treated as a constant. Experimental data suggests ϵ_t is negligible for saltating load [*Sklar and Dietrich*, 2001], and therefore ϵ_t is taken as zero for this study.

Sklar and Dietrich [2004] use the vertical component of impact velocity(w_{si}), where the subscript s refers to the saltating sediment grain and the subscript i indicates impact with the bed, to characterize the energy transferred to the bed, rather than v_n. Therefore, *Sklar and Dietrich* [2004] combine Eqs. 2.2 and 2.3 to calculate V_i as

$$V_i = \frac{\pi \rho_s D_s^3 w_{si}^2 Y}{6 k_v \sigma_T^2} \tag{2.4}$$

where $\pi \rho_s D_s^3 v_n^2 / 6 = 2K_p$, ρ_s is the density of sediment, and D_s is grain diameter.

2.1.2 Saltation Characteristics

Sklar and Dietrich [2004] develop empirical expressions for average saltation hop length and height based on analysis of nine previous experimental and theoretical studies of saltation. Instead of accounting for the various forces on individual saltating grains, these regressions of published data constitute a self-consistent description of how saltation trajectories vary as a function of flow strength and grain size. This approach is continued here for consistency with *Sklar and Dietrich* [2004].

Saltation hop height is best fit by

$$H_s = 1.44 D_s \left(\frac{\tau^*}{\tau_c^*} - 1 \right)^{0.50} \tag{2.5}$$

where τ^* is the nondimensional form of the boundary shear stress (τ_b), defined as

$$\tau^* = \frac{\tau_b}{(\rho_s - \rho_w) g D_s} \tag{2.6}$$

and τ_c^* is the value of τ^* at the threshold of particle motion, ρ_w is the density of water, and g is gravitational acceleration. *Sklar and Dietrich* [2004] use a critical value of nondimensional boundary shear stress of $\tau_c^* = 0.03$. The ratio τ^*/τ_c^* is known as the transport stage, and represents flow strength. Regressions are written as functions of nondimensional excess shear stress $(\tau^*/\tau_c^* - 1)$ to account for the reduced intensity of particle motion at low excess shear stresses, and to force zero sediment transport at $\tau^* = \tau_c^*$. By definition, there is no transport when $\tau^* < \tau_c^*$.

Similarly, average saltation hop length is predicted by

$$\overline{L_s} = 8.0 D_s \left(\frac{\tau^*}{\tau_c^*} - 1 \right)^{0.88} \tag{2.7}$$

where the overbar indicates a mean quantity. Later, with the introduction of turbulence, L_s will vary around $\overline{L_s}$. While Eqs. 2.5 and 2.7 give information on total saltation hop length and height, the shape of the trajectory is not defined. *Hu and Hui* [1996b] report measurements of total hop length (L_s) and ascending hop length (L_{su}) that indicate a linear relationship, approximated as $L_{su} = \frac{1}{3}\overline{L_s}$. Therefore, the descending portion of the trajectory has average length

$$\overline{L_{sd}} = {}^{2}/{}_{3}\overline{L_s} \ . \tag{2.8}$$

Sklar and Dietrich [2004] use this ⅔ factor in estimating the vertical impact velocity (see Eq. 2.9 below).

2.1.3 Vertical Impact Velocity (w_{si})

None of the studies analyzed by *Sklar and Dietrich* [2004] include direct measurements of the vertical component of impact velocity (w_{si}). However, *Sklar and Dietrich* [2004] argue that the mean sediment particle descent velocity (w_{sd}) can be written as

$$w_{sd} = 0.4(R_b g D_s)^{1/2}\left(\frac{\tau^*}{\tau^*_c} - 1\right)^{0.18} \tag{2.9}$$

where $R_b = \rho_s/\rho_w - 1$ is the nondimensional buoyant density of sediment. Using data from *Abbott and Francis* [1977] and *Wiberg and Smith* [1985], *Sklar and Dietrich* [2004] estimate that on average, the vertical velocity when the particle reaches the same elevation as takeoff ($\overline{w_{sf}}$) is

$$\overline{w_{sf}} \approx 2w_{sd} \ . \tag{2.10}$$

As with $\overline{L_s}$, the overbar indicates a mean quantity around which w_{sf} will vary with the introduction of turbulence. *Sklar and Dietrich* [2004] use $\overline{w_{sf}}$ as an estimate of w_{si} for their case of flat topography. Here, w_{sf} is used as part of an estimate of v_n.

2.1.4 Exposed Fraction (F_e)

The exposed fraction of the bed defines the proportion of saltation impacts that can actually remove volume. *Sklar and Dietrich* [2004] define F_e as

$$F_e = 1 - \frac{q_s}{q_t} \tag{2.11}$$

for $q_t \geq q_s$, and $F_e = 0$ if $q_s > q_t$, where q_s is the sediment mass flux per width and q_t is the stream's sediment transport capacity per width. *Sklar and Dietrich* [2004] use the *Fernandez-Luque and van Beek* [1976] bed load sediment transport relation to define q_t,

$$q_t = 5.7\rho_s(R_b g D_s^3)^{1/2}(\tau^* - \tau_c^*)^{3/2} \ . \tag{2.12}$$

While a linear description of the cover effect is simple and straightforward, other formulations of F_e have been proposed. For example, *Turowski et al.* [2007] present an exponential model from a probabilistic argument. This model of F_e has been implemented with success [*Turowski et al.*, 2008]. More realistically, *Hancock and Anderson* [2002] suggest the thickness of the alluvial cover is important to determining the exposed fraction. This approach allows changes in sediment load through the river's history to affect the extent of alluvial cover in the future, and reflects the reality of the situation much better than a ratio of sediment flux to transport capacity. However, for consistency with *Sklar and Dietrich* [2004], Eq. 2.11 is used here.

2.1.5 Impact Rate (I_r)

The rate of saltation impacts on the bed, per unit area and per unit time (I_r), is proportional to the flux of bed load particles and inversely proportional to the downstream distance between impacts. Therefore, *Sklar and Dietrich* [2004] write the impact rate as

$$I_r = \frac{6q_s}{\pi\rho_s D_s^3 \overline{L_s}} \ . \tag{2.13}$$

2.2 Modifications to the Model

By introducing topography, it becomes important to explicitly define the saltation trajectory to determine sediment impact locations and impact characteristics. With non-flat topography, the angle at which the grain impacts the topography becomes relevant (ξ - see Fig. 2.2), and the normal impact velocity (v_n) must replace the vertical impact velocity (w_{si}) in Eq. 2.4. Since this velocity is squared, the difference between w_{si} and v_n is significant in determining V_i on non-flat surfaces. Similarly, the downstream distance traveled during a single hop can be greater than or less than $\overline{L_s}$, as shown by the various trajectories in Fig. 2.2. Here, the hop trajectory and v_n are defined more completely.

2.2.1 Topography

Sklar and Dietrich's [2004] model applies strictly to sections of streams with flat, horizontal beds. The modified model presented here, however, is applied to simple repeating topography – a topographic rise with constant slopes (see Fig. 2.2). The bump is defined by the angle of its flow-facing slope (θ), its total length (l), and the horizontal length of the flow-facing slope (l_{up}). The analysis presented here relies on the base case with $l = 50$ cm, $l_{up} = 5$ cm, and $\theta = 30°$. The sensitivity to these parameters are analyzed in Sec. 3.3.

The topography is repeating, such that a saltating grain will continually encounter identical terrain as it moves downstream. The scale of the topography is much larger than the sediment grains ($D_s = 1 - 20$ mm), allowing saltating grains to be treated as point particles. Additionally, the topography is small compared to flow depth, allowing for the assumption that the topography does not greatly affect the flow, as is the case for topography on the scale of alluvial cover on the bed. This assumption is evaluated in Chapter 4. Finally, the slope of the channel is negligible.

2.2.2 Trajectory

It is assumed that topography does not impact the flow enough to change basic saltation hop characteristics (e.g. $\overline{L_s}$, H_s, $\overline{w_{sf}}$). Saltation trajectories are simulated using cubic splines [*D'Errico*, 2009]. Trajectories are forced to go through the takeoff point, a point L_{su} downstream of takeoff and H_s above takeoff, and a point $\overline{L_s}$ downstream of takeoff and at the takeoff elevation. Furthermore, trajectories are forced to be concave down and have negative curvature. Modeled trajectories using these parameters fit very well with published trajectories [*Hu and Hui*, 1996a], as shown in Fig. 2.1. The takeoff angle (ψ) is defined by $\frac{\partial z}{\partial x}\big|_{x=0}$, where z and x are the vertical and horizontal positions of the saltating grain, respectively.

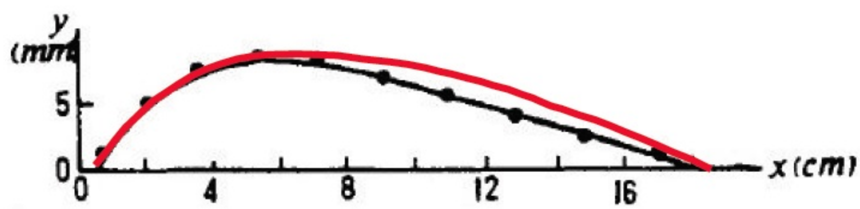

Figure 2.1: Measured trajectory (black line) from *Hu and Hui* [1996a] and modeled trajectory (red line) given H_s, L_s, and L_{su} using cubic splines.

2.2.3 Combining Saltation and Topography

In the most basic sense, each simulated saltation hop takes off from one point on the given topography and lands at another, eroding a small volume from the surface according to Eq. 2.4. However, determining the impact location is not as simple as adding $\overline{L_s}$ to the takeoff location due to changes in elevation between takeoff and impact. Therefore, the impact characteristics cannot be determined by the model presented by *Sklar and Dietrich* [2004].

Because the topography is large compared to the saltation trajectories, impacts can occur on both the ascending and descending portions of the trajectory (Fig. 2.2). The differences in impact characteristics this creates are discussed below.

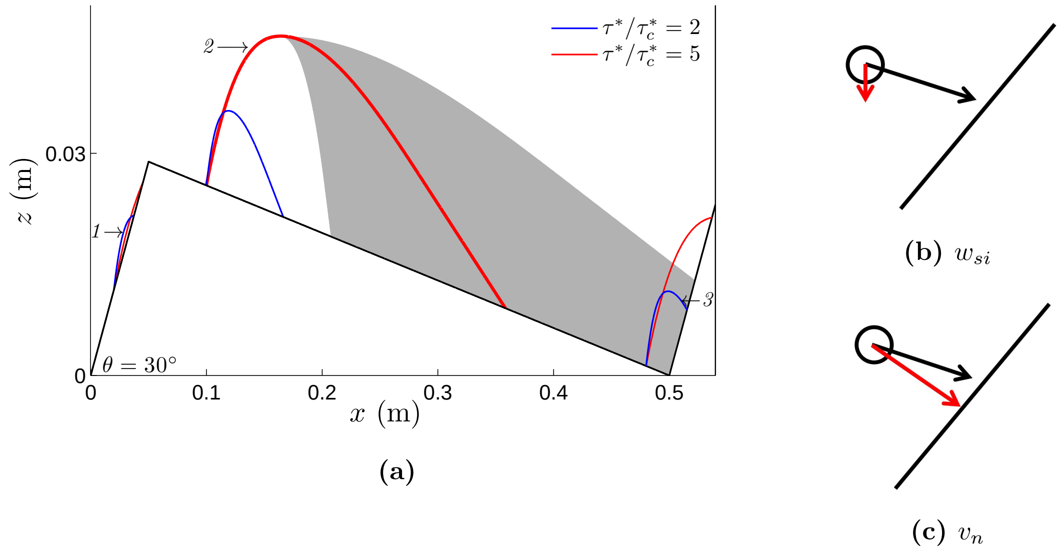

Figure 2.2: (a) Sample trajectories for $D_s = 7$ mm at two different flow strengths from three takeoff locations over topography defined by $\theta = 30°$, $l_{up} = 0.05$ m and $l = 0.5$ m (Vertical exaggeration ≈ 6.5). Given turbulence, trajectory *2* could fall anywhere within shaded region (See Sec. 2.2.5). Schematic of (b) w_{si} vs. (c) v_n, where the black arrow is the velocity of the particle impinging on the surface (black line) on a trajectory like *3* from (a), and the red arrow represents w_{si} and v_n, respectively.

2.2.4 Impact Characteristics

Saltating grains can impact the bed topography while they are either descending or ascending. While the physics of these impact scenarios are identical, the components of impact velocity must be determined differently depending on whether the impact occurs on the particle's ascent or descent.

2.2.4.1 Descending Case

It has been shown that horizontal velocity of a saltating grain along its descent is nearly constant [*Hu and Hui*, 1996a]. For example, in the trajectory shown in Fig. 2.1, the horizontal velocity of the particle changes by less than 5% along the descent [*Hu and Hui*, 1996a]. This constant velocity can be determined by geometry, as

$$\frac{\overline{w_{sf}}}{u_{sd}} = -\frac{\partial z}{\partial x}\bigg|_{x=\overline{L_s}} \tag{2.14}$$

where u_{sd} is the horizontal velocity of the saltating particle along its descent. The spatial derivative $(\partial z/\partial x)$ is known at all x, allowing for simple evaluation of Eqs. 2.14 and 2.15.

The horizontal impact velocity (u_{si}) is taken to be equal to u_{sd} along the descent. Extending Eq. 2.14 to the case of impact, the vertical impact velocity (w_{si}) is taken as

$$w_{si} = -u_{si} \left.\frac{\partial z}{\partial x}\right|_i . \tag{2.15}$$

The negative signs in Eqs. 2.14 and 2.15 reflect that a positive vertical particle velocity (w_s) is in the $-z$ direction. Since $z(x)$ has negative curvature, Eq. 2.15 implies that hops shortened by topography will impact with slower vertical velocities than predicted by *Sklar and Dietrich* [2004], hops that impact at the same elevation as takeoff will have vertical velocities equal to those predicted by *Sklar and Dietrich* [2004], and hops that are lengthened due to topography will impact faster in the vertical than predicted by *Sklar and Dietrich* [2004]. These vertical impact velocities will not be much greater than those predicted by *Sklar and Dietrich* [2004] since $\partial z/\partial x$ does not change much when z is below takeoff elevation.

2.2.4.2 Ascending Case

For the case in which a saltating grain impacts the bed while it is still rising along its trajectory, like trajectory *1* in Fig. 2.2, a different set of equations are needed to determine the impact characteristics. *Sklar and Dietrich*'s [2004] data analysis show the average horizontal particle velocity over the duration of a hop that takes off and lands at the same elevation is

$$\overline{u_s} = 1.56(R_b g D_s)^{1/2} \left(\frac{\tau *}{\tau_c^*} - 1\right)^{0.56} . \tag{2.16}$$

For this condition to be true while Eq. 2.15 is also true, then along the ascent,

$$u_{su} = 3\overline{u_s} - 2u_{sf} \tag{2.17}$$

where u_{su} is the horizontal velocity of the particle along its ascent. As in the descending case, $u_{si} = u_{su}$ along the ascent. The vertical impact velocity is solved for using Eq. 2.15. Compared to observations, this estimate of u_{su} might be slow, but it is geometrically consistent.

2.2.4.3 Normal Impact Velocity (v_n)

While expressions for w_{si} and u_{si} are relatively easy to obtain, Eq. 2.4 requires an estimate of v_n. The component of impact velocity normal to the surface requires knowledge about the impact speed (S_i) and impact angle (ξ). Since w_{si} and u_{si} are orthogonal, S_i is

$$S_i = \sqrt{w_{si}^2 + u_{si}^2} \ . \tag{2.18}$$

If ξ is considered the angle between the bedrock surface and the particle trajectory, then v_n is

$$v_n = S_i \sin \xi \ . \tag{2.19}$$

2.2.5 Introducing Variability

Simulating individual saltation hops using the previously defined equations requires identical hop trajectories for grains of equal size. Obviously, this is not the case in nature. The randomness of turbulence in streamflow drives this variability. *Lamb et al.* [2008] expand on *Sklar and Dietrich*'s [2004] model to include turbulence. In this approach, a normal distribution is applied to w_{sf} to account for vertical fluctuations in the flow field. These fluctuations have standard deviation approximately equal to the friction velocity (u_*) [*Nezu and Nakagawa*, 1993]. Therefore, each hop has w_{sf} defined by

$$w_{sf} = \overline{w_{sf}} + w' \tag{2.20}$$

where $\overline{w_{sf}}$ is defined by Eq. 2.10, and w' is a random number from a truncated normal distribution with mean zero and standard deviation u_*, such that $-\overline{w_{sf}} < w' \leq 6u_*$ [*Lamb et al.*, 2008]. The friction velocity is defined by $u_* = (\tau_b/\rho_w)^{1/2}$ [*Sklar and Dietrich*, 2004].

This variability in w_{sf} forces variability in L_{sd}; an increase in w_{sf} means that the saltating grain will fall from H_s more quickly. This more rapid fall necessarily decreases L_{sd}.

Descending hop length deviates from $\overline{L_{sd}}$ as

$$L_{sd} = \frac{\overline{w_{sf}}}{w_{sf}} \overline{L_{sd}} \quad . \tag{2.21}$$

Other saltation characteristics (e.g. u_{si}, S_i, v_n) are defined by Eqs. 2.14, 2.18, and 2.19 using the deviatoric quantities w_{si} and L_{sd} from Eqs. 2.20 and 2.21. Saltation characteristic quantities H_s and L_{su} are unaffected by w'.

2.2.6 Impact Rate (I_r)

With topography, the actual average length of each saltation hop is not $\overline{L_s}$. Therefore, it does not make sense to calculate impact rate according to Eq. 2.13. Instead, the impact rate per unit area is calculated through the simulation of n successive hops, representing a population of particles traversing the topography with takeoff points spanning the domain. With the assumption that while ascending, the grain travels with horizontal velocity u_{su} (defined by Eq. 2.17), and at u_{sf} (defined by Eq. 2.14) while descending, the total time (t_{tot}) and total distance traveled (s_{tot}) are calculated. These quantities can be broken into time spent and distance traveled above the upslope (t_u, s_u) and downslope (t_d, s_d). The simulation is further assumed to have unit width ($W = 1$). With this assumption, distances can be transformed to areas traversed (A_{tot}, A_u, A_d).

Impact rates are calculated on the upslope as

$$i_u = \frac{n_u}{t_u A_u} \tag{2.22}$$

where n_u is the number of impacts on the upslope. A similar quantity i_d is calculated using corresponding quantities for the downslope. To extend i_u and i_d to impact rates for a section of stream with a known sediment flux per width q_s, the mass flux per particle per width (m) is calculated as

$$m = \frac{\pi \rho_s D_s^3}{6 t_{tot} W} \quad . \tag{2.23}$$

Therefore, the particle flux per width is q_s/m, and total impact rates per width for the upslope can be calculated as

$$I_{r,u} = i_u \frac{q_s}{m} \ . \tag{2.24}$$

An impact rate for the downslope ($I_{r,d}$) is similarly calculated. These impact rates are used in Eq. 2.1 to determine incision rates along the upslope and downslope (E_u, E_d). An estimate of the net erosion rate along the entire domain (E) is made using a weighted average of E_u and E_d. That is,

$$E = \frac{l_{up}}{l} E_u + \left(1 - \frac{l_{up}}{l}\right) E_d \tag{2.25}$$

where l_{up} is the horizontal distance covered by the upslope ($l_{up} = h \cot \theta$).

2.3 Model Algorithm

The model acts by simulating a single saltating grain traversing the topography several times given a wrap-around boundary condition. The number of simulated hops (n) are specified, as are the quantities related to sediment and bed characterization, topography, and flow strength. The particle is assigned a random initial location. For each hop, H_s is assigned by Eq. 2.5, and L_s is assigned by Eqs. 2.7 and 2.21. A trajectory is fitted to the assigned points, and the intersection between topography and the fitted trajectory is found. From this point, impact characteristics are determined and an eroded volume (V_i) is calculated. Throughout the trajectory, the particle's horizontal velocity and position are tracked to create measurements of time traversing both the upslope and downslope (t_u, t_d).

Chapter 3

Results

An example model run can be used to examine the distribution of n impacts over the topography, as well as produce single values of E, E_u, and E_d over the domain. Both types of output are instructive, informing where erosion is focused as well as the rate of erosion.

3.1 Eroded Volume per Impact

Results of the model show that grain-bed impacts fall clearly into three categories (See Table 3.1). First, there are impacts on the downslope that all occur on the particle's descent. These impacts are fairly low-angle and have a small normal velocity. For the base case, where $D_s = 5$ mm, $\tau^*/\tau_c^* = 4$, $\theta = 30°$, $l = 0.50$ m, and $l_{up}/l = 0.1$, these impacts are characterized by $\xi < 35°$ and $v_n < 0.25$ m s^{-1}. Second, there are impacts on the upslope along the particle's ascent. These impacts are also low angle with low normal velocity. For the case above, these impacts also occur with $\xi < 35°$, with a slightly higher range of v_n, up to about 0.5 m s^{-1}. In the third category, where impacts occur on the descent along the upslope, eroded volume per impact is greater than the other categories due to greater normal velocities and impact angles (for the base case, $\xi > 35°$ and $v_n > 0.5$ m s^{-1}). Schematics of these trajectories can be seen in Fig. 2.2. While this third category has proportionately fewer impacts, these impacts dominate the erosive record. In the base case, 21% of the impacts account for 75% of the total eroded volume.

The spatial distribution of V_i (Fig. 3.1) shows the impacts that remove the most volume

Table 3.1: Model output summary for case with $l = 0.5$ m, $l_{up}/l = 0.1$, $\theta = 30°$, $D_s = 5$ mm, τ^*/τ_c^*

Category	V_i ($\times 10^{-14}$ m^3) 5% – 95%	v_n (m/s) 5% – 95%	ξ (°) 5% – 95%	% impacts	% Erosion
downslope	0.15 – 2.57	0.093 – 0.381	5.1 – 19.8	49.6	22.7
upslope ascend	0.03 – 0.29	0.042 – 0.129	5.4 – 18.3	29.3	2.3
upslope descend	5.18 – 12.78	0.541 – 0.850	31.7 – 50.5	21.1	75.0

($V_i > 0.5 \times 10^{-13}$ m^3) are located on the upslope. These impacts represent the third category (descending on upslope). The upslope impacts associated with relatively low eroded volume ($V_i < 0.1 \times 10^{-13}$ m^3) represent the second category (ascending on the upslope). In Fig. 3.1, the area with no impacts (between 0.05 and approx. 0.10 m) represents a shadow zone, where particles taking off on the upslope cannot land due the geometry of their trajectories. The lens of no impacts within the swath of downslope impacts represents the difference between the two major type of downslope impacts. Impacts to the left of the lens represent particles that have hopped up over the crest of the bump, whereas impacts downstream of the lens represent particles that have taken off from the downslope and landed further downstream.

Saltating particles that erode large volumes impact the bed with high normal velocities, as V_i scales with the square of v_n (see Eq. 2.4). High normal velocity can be due to either a high speed at impact or an impact angle approaching perpendicularity (see Eq. 2.19). The interplay between V_i, v_n, and ξ is shown in Fig. 3.2. The three impact types are again clear, with impacts associated with high eroded volume occuring along the upslope at high angles and normal velocities.

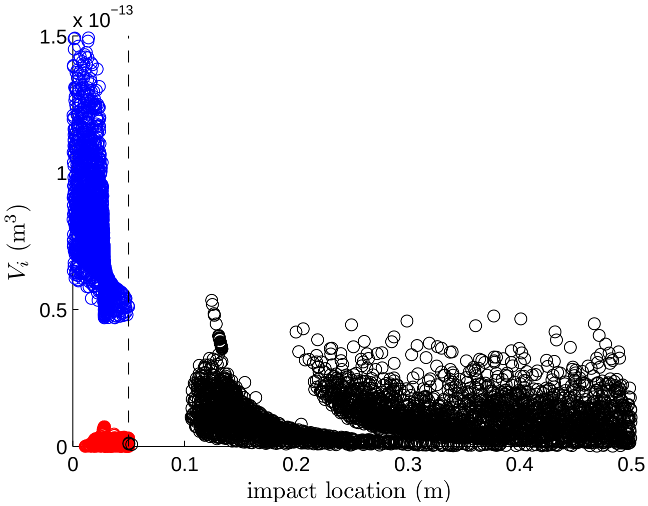

Figure 3.1: Spatial distribution of V_i for a model run with $D_s = 5$ mm, $\tau^*/\tau_c^* = 4$, $\theta = 30°$, $l = 0.5$ m, $l_{up}/l = 0.1$. Points in blue represent impacts along the upslope that occur during the particle's descent. The cluster of upslope impacts with relatively low V_i represent impacts along the ascent are shown in red.

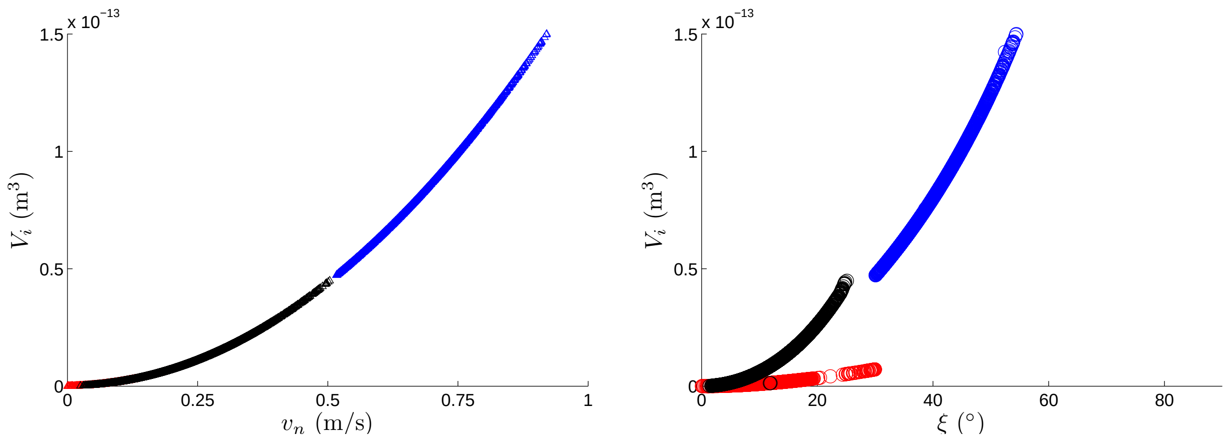

(a) **(b)**

Figure 3.2: V_i as a function of (a) v_n and (b) ξ for a model run with $D_s = 5$ mm, $\tau^*/\tau_c^* = 4$, $\theta = 30°$, $l = 0.5$ m, $l_{up}/l = 0.1$. Points in blue represent descending impacts on the upslope, red points represent ascending impacts along the upslope, and black points represent impacts on the downslope.

3.2 Erosion Rates

In the geomorphic sense, however, the eroded volume per impact is important mainly in characterizing the rates of erosion in the channel. Combining the V_i record with calculated impact rates (I_r) and the exposed fraction of the bed (F_e) allows calculation of an erosion rate (E) that determines how quickly the bed is lowered (Eq. 2.1). The model requires certain parameters to characterize the bed as well as the sediment flux downstream. Here, values used are meant to approximate a gauged reach of the South Fork Eel River, California, and are taken from *Sklar and Dietrich* [2004] (See Table 3.2).

Table 3.2: Model parameter input values corresponding to the South Fork Eel River, California

Input	Symbol	Value	
Sediment Supply	Q_s	42.6	kg/s
Channel Width	W	18.0	m
Rock tensile strength	σ_T	7.0	MPa
Rock elastic modulus	Y	5.0×10^4	MPa
Dimensionless rock resistance parameter	k_v	1.0×10^6	
Sediment density	ρ_s	2650	kg/m^3
Water density	ρ_w	1000	kg/m^3
Channel Slope	Φ	0.0053	
Discharge	Q_w	39.1	m^3/s
Manning's roughness	n_m	0.035	

The effect of topography on erosion can be shown by comparing erosion rates on both the upslope (E_u) and over the domain (E) to the case where erosion occurs on flat topography (E_f). In a given flow, the influence of topography on erosion rates is dependent upon the saltating grain size. Figure 3.3 shows erosion enhancement (E_u/E_f, E/E_f) as a function of D_s. Smaller grain sizes lead to greater enhancement of erosion, indicating that bed topography is more important for streams with bed load dominated by smaller grain sizes.

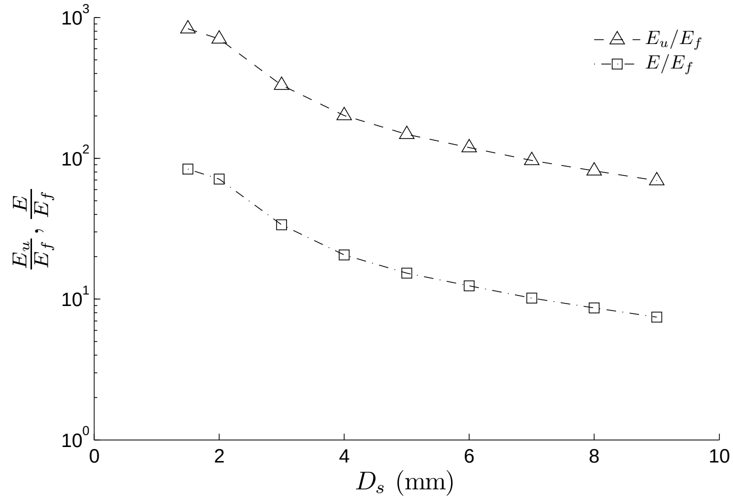

Figure 3.3: Erosion enhancement as a function of D_s for a flow with $\tau_b = 9.71$ Pa, $q_s = 0.237$ kg m^{-1} s^{-1}. $l = 0.5$ m, $l_{up}/l = 0.1$, $\theta = 30°$.

The effects of topography can be seen most directly in Figs. 3.4 and 3.5, where E is shown as a function of τ^*/τ_c^* and D_s, respectively. Erosion rates increase strongly with increasing flow strength and decrease with increasing grain size (red lines). This result is starkly opposed to the behavior of E over smooth, flat terrain (black lines). Over flat terrain, E peaks at moderate grain sizes and moderate flow strengths [*Sklar and Dietrich*, 2004]. In Figs. 3.4 and 3.5, D_s and τ^*/τ_c^* values were specifically chosen to match corresponding E vs. τ^*/τ_c^* and E vs. D_s plots from *Sklar and Dietrich* [2004]. It is clear that the introduction of bed topography has significant effect on modeled erosion rates beyond simply increasing the amount. The effects of flow and grain size are different in the case with topography and the flat case.

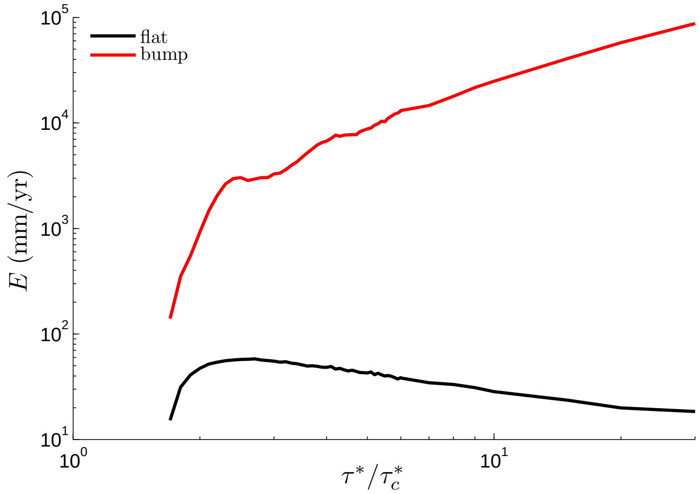

Figure 3.4: Inclusion of topography results in enhanced erosion rates E that increase with increasing τ^*/τ_c^*, versus peaking at moderate τ^*/τ_c^* given a flat bed. $D_s = 60$ mm, $l = 0.5$ m, $l_{up}/l = 0.1$, $\theta = 30°$.

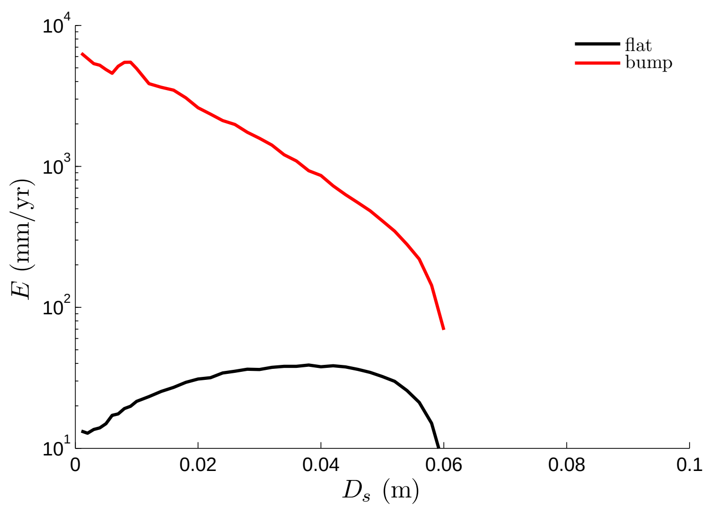

Figure 3.5: Inclusion of topography results in enhanced erosion rates E that decrease with increasing D_s, versus peaking at moderate D_s given a flat bed. $\tau_b = 48.6$ Pa, $l = 0.5$ m, $l_{up}/l = 0.1$, $\theta = 30°$.

3.3 Sensitivity Analysis

The above analysis relies on a specific geometry to determine the effect of topography. To evaluate how the geometry of the topography affects the results, the sensitivity of the model to changes in θ is tested. To illustrate the effect of θ on erosion enhancement (E/E_f), the model was run at a fixed grain size and flow strength for θ values between 0° and 90°, keeping the height of the bump equal for all runs (see Fig. 3.6). These results are presented in Fig. 3.7.

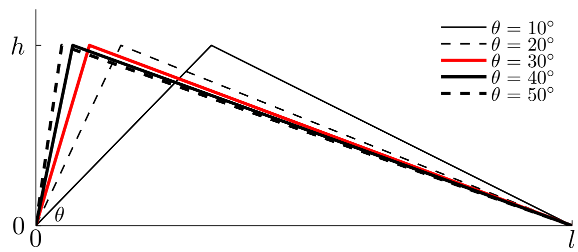

Figure 3.6: Topography with varying θ. Height is kept constant at 0.029 m, and the total length is kept constant at $l = 0.50$ m.

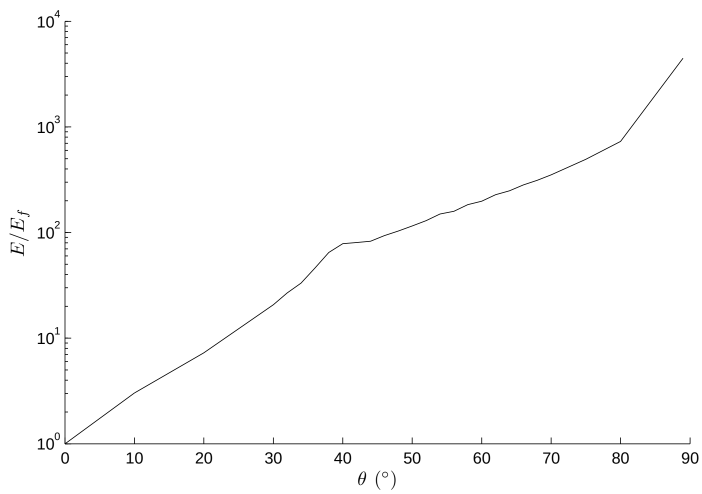

Figure 3.7: Effect of θ on erosion enhancement (E/E_f). $D_s = 4$ mm, $\tau^*/\tau_c^* = 5$, $q_s = 0.237$ kg m^{-1} s^{-1}. For all nonzero θ, the bump height is equal to 0.029 m. For all cases, $l = 0.5$ m.

Erosion enhancement increases monotonically with θ. The steeper the slope, the greater the erosion enhancement due to topography. As the slope becomes steeper, u_{si} plays a larger role in determining v_n. Since u_{si} is several times greater than w_{si}, maximizing the energy transferred to the bed by downstream motion of saltating grains will maximize erosion rates.

This trend of increasing E with increasing θ is consistent across a range of grain sizes or flow strengths. Regardless of θ, the trends of E decreasing with D_s and increasing with τ^*/τ_c^* are apparent (Fig. 3.8). Thus, the main differences between this study and *Sklar and Dietrich* [2004] do not depend on θ.

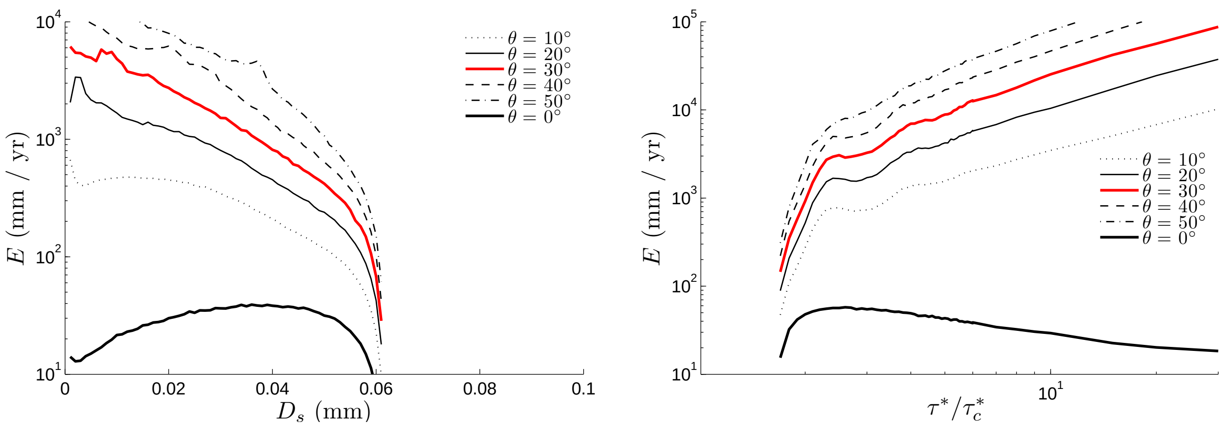

(a) **(b)**

Figure 3.8: Effect of θ on E with varying (a) D_s for a flow with $\tau_b = 48.6$ Pa and (b) varying τ^*/τ_c^* with $D_s = 60$ mm grains. For all nonzero θ, the bump height is equal to 0.029 m. For all θ, $l = 0.5$ m.

It is also clear from Fig. 3.8 that any bed topography, no matter how gentle, greatly increases erosion rate. This shows that whenever the downstream particle velocity (u_{si}) transfers energy to the bed, erosion rates are greatly enhanced.

Chapter 4

Discussion

The results demonstrate that by incorporating bed topography into the saltation-abrasion model, maximum erosion occurs with small grain size and strong flows. This is directly opposed to maximal erosion occuring with medium-sized grains and moderate flows, as proposed by *Sklar and Dietrich* [2004] for transport over smooth, flat stream beds. Both the model presented here and saltation-abrasion model presented by *Sklar and Dietrich* [2004] are extensively simplified representations of nature. The implications of some of the prominent simplifications are discussed here.

4.1 Effect of Topography on Flow

One of the underlying assumptions of this study is that the stream bed topography does not affect the overlying flow. In rapidly varying open channel flow, friction is typically neglected [*Chow*, 1959; *Chaudhry*, 1993]. Assuming a rectangular channel cross-section (as do *Sklar and Dietrich* [2004]), flow over a bump in the channel can be described by the Bernoulli principle,

$$\frac{Q_w^2}{2gW^2H_{w1}^2} + H_{w1} = \frac{Q_w^2}{2gW^2H_{w2}^2} + H_{w2} + \Delta b \tag{4.1}$$

where Q_w is the stream discharge, W is channel width, H_{w1} and H_{w2} are the height of water before and at the bump, respectively, and Δb is the height of the bump.

Sklar and Dietrich [2004] assert that τ_b can be calculated as

$$\tau_b = \rho_w g R_H \Phi \tag{4.2}$$

where Φ is the mean channel slope, and R_H is the hydraulic radius, which can be found using the Manning equation for mean flow velocity as

$$R_H = \left(\frac{Q_w n_m}{H_w W \Phi^{1/2}} \right)^{3/2} \tag{4.3}$$

where n_m is the Manning's roughness coefficient. Substituting Eqs. 4.2 and 4.3 into Eq. 2.6,

$$\tau^* = \left(\frac{Q_w n_m}{H_w W \Phi^{1/2}} \right)^{3/2} \frac{\rho_w \Phi}{(\rho_s - \rho_w) D_s} . \tag{4.4}$$

Sklar and Dietrich [2004] define all flows by normalized shear stress corresponding to a grain size D_s, where $\tau_c^* = 0.03$ is taken as constant. Natural flows are all subcritical, that is, their Froude number ($Fr = u/\sqrt{gH_w}$) is less than unity. The Froude number can be equivalently defined as $Fr = (h_c/H_w)^{3/2}$ where h_c is a critical flow depth equal to $(Q_w^2/gW^2)^{3/2}$. This value of H_w corresponds to a minimum value of the left side of Eq. 4.1. Therefore, for a flow to be subcritical there is a maximum possible value of τ^*/τ_c^* for each D_s corresponding to $H_w = h_c$,

$$\left[\frac{\tau^*}{\tau_c^*} \right]_{max} = \left[\frac{Q_w n_m}{\left(\frac{Q_w^2}{gW^2} \right)^{1/3} W \Phi^{1/2}} \right]^{3/2} \frac{\rho_w \Phi}{(\rho_s - \rho_w) D_s \tau_c^*} . \tag{4.5}$$

Similarly, there is a maximum bump height for every flow that will keep the flow from transitioning into supercritical state ($Fr > 1$). This is calculated from Eq. 4.1 where $H_{w2} = h_c$, as

$$\Delta b_{max} = \frac{Q_w^2}{2gW^2 H_{w1}^2} + H_{w1} - \frac{Q_w^2}{2gW^2 h_c^2} - h_c \tag{4.6}$$

where H_{w1} is defined by rearrangement of Eq. 4.4. Parameter values necessary for these calculations are presented in Table 3.2, and again correspond to the South Fork Eel River, California [*Sklar and Dietrich*, 2004]. The maximum bump height for several grain sizes across a range of flow strengths is shown in Fig. 4.1.

It is clear that in the base case, where $\tau_b = 9.71$ Pa ($D_s = 5$ mm, $\tau^*/\tau_c^* = 4$), and the bump has height 0.029 m ($l = 0.5$ m, $l_{up}/l = 0.1$, $\theta = 30°$), the height of the bump will not cause the flow to transition to a supercritical state. It would take a bump more than ten times taller to affect the criticality of the flow. Additionally, this size bump will not will not cause transition to supercriticality for a flow with $\tau_b = 48.6$ Pa (Figs. 3.5 and 3.8a).

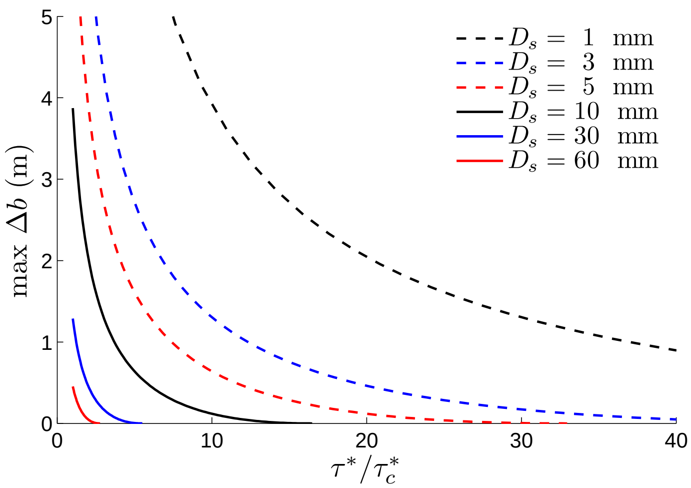

Figure 4.1: Maximum bump height for six grain sizes across a range of flow strengths.

As long as the bump height is small enough relative to the flow depth, then the topography will not substantively affect the flow. Obviously, smaller bumps will have a smaller effect than larger bumps in the same flow. However, streamlines will be compressed, changing the flow field close to the bed. The details of the velocity structure are not compensated for in the proposed model.

If the bump height is great enough and the angle of the bump steep enough, however, flow separation can be induced. Flow separation will tend to increase the effect of suspended load on the bed, as suspended sediment will be driven down into the lee side of the bump, creating structures like potholes [e.g. *Hancock et al.*, 1998; *Whipple et al.*, 2000; *Wilson et al.*, 2013].

4.2 Effect of Topography on Impact Characteristics

Despite not substantively affecting the flow, a topographic bump will cause the flow to accelerate (see Eq. 4.1) over the stoss side irregularity and decelerate over the lee side. This will affect the three types of impacts (Table 3.1) in different ways. Impacts on the downslope will impact the bed at steeper than calculated angles as the flow decelerates on the lee side of the bump. The deceleration of the flow may also result in the grain impacting the bed with slower than calculated speeds. These two effects alter V_i in opposite directions.

Impacts on the upslope stoss side of the bump while the grain is ascending will be accelerated by the flow over the bump. This will cause the impacts to occur at a smaller angle, but a greater speed. Again, the effects of changes in ξ and S_i on V_i will oppose each other. In any case, this type of impact accounts for a very small percentage of the total erosion, so any changes will not greatly affect the results.

Finally, accelerating flow over the stoss side of the bump will tend to shallow out saltation trajectories that result in impacts that occur on the upslope during a particle descent. This implies a reduction in ξ that would tend to reduce V_i. However, the faster flow may cause the impact to occur at a greater speed S_i, which would tend to increase V_i. Again, the two effects will act against each other. Since these types of impacts account for a majority of erosion deviation from calculated values will have the greatest effect on this category. The relative importance of changes in S_i and ξ will depend on the flow strength and grain size. Larger particles will be less affected by changes in the flow than smaller particles [*Anderson*, 1986].

For all impacts, the flow accelerating over the bump will cause deviation from the calculated values of impact angle and speed. These deviations, however, oppose each other, implying that the overall effect on V_i and therefore E will be small. The main results of the study are still valid – erosion by bed load is greatest at high flows and with smaller grains.

4.3 Particle Velocity Profiles

The horizontal velocity profile applied to the saltating grains (Eqs. 2.14 and 2.17) is defined in a piecewise fashion, and therefore does not represent the physical system very well. There is no perfect solution to this problem; there is not enough known information to adequately estimate a saltating grain's horizontal velocity at all points along its trajectory. Another possible solution would be to assign $u_s = \overline{u_s}$ at all points along the trajectory, where $\overline{u_s}$ is defined by Eq. 2.16. When this is done, the changes E are minimal, as the difference between $\overline{u_s}$ and u_{sf} is small, and the effect of particle impacts on the upslope are negligible (Table 3.1). Using $\overline{u_s}$ does not change the trends seen.

4.4 Use of Regression Statistics

In this study, regressions relating nondimensional excess shear stress to saltation characteristics from *Sklar and Dietrich* [2004] are used to simulate saltation trajectories and impacts. *Sklar and Dietrich* [2004] specifically note that their model does not simulate specific trajectories, and instead use their regressions of data from several other saltation studies to capture average characteristics of saltating grains. Still, simulating trajectories from average characteristics will capture the average behavior of saltating grains. The approach presented here will effectively simulate the effect of saltating bed load over bed topography.

The regressions from *Sklar and Dietrich* [2004] rely on data from nine studies of saltation trajectory. Only one of these studies used grains larger than 10 mm [*Niño et al.*, 1994]. While *Sklar and Dietrich* [2004] use these regressions for larger grains ($D_s = 60$ mm), the data used to create these regressions does not extend that far. The validity of the model decreases as grains get larger than approximately 10 mm. For this reason, the base case in this study uses $D_s = 5$ mm, which is firmly in the middle of the grain sizes used in the studies used to create the regressions.

4.5 Distribution of F_e

Here, alluvial cover is treated as uniformly distributed across the streambed. By doing so, the cover effect can be accounted for using a single parameter (F_e). In reality, the alluvial cover will most likely exist as patches in topographic lows. This cover will reduce the number of impacts on both the upslope and the downslope at a ratio approximately equal to the ratio of their horizontal lengths. This means that the distribution of the alluvial cover will not greatly affect erosion rates, and treating F_e as a uniform random distribution of patches is a valid method of calculating E.

4.6 Agreement with Experimental Results and Field Observations

In addition to showing that bed topography increases erosion rates, the results show that this erosion is focused on flow-facing slopes (Figs. 3.1 and 3.3). This finding is supported by results from flume experiments (see Fig. 4.2) [*Johnson and Whipple*, 2010], and observations in the field [*Whipple et al.*, 2000; *Johnson and Whipple*, 2007; *Goode and Wohl*, 2010; *Wilson et al.*, 2013].

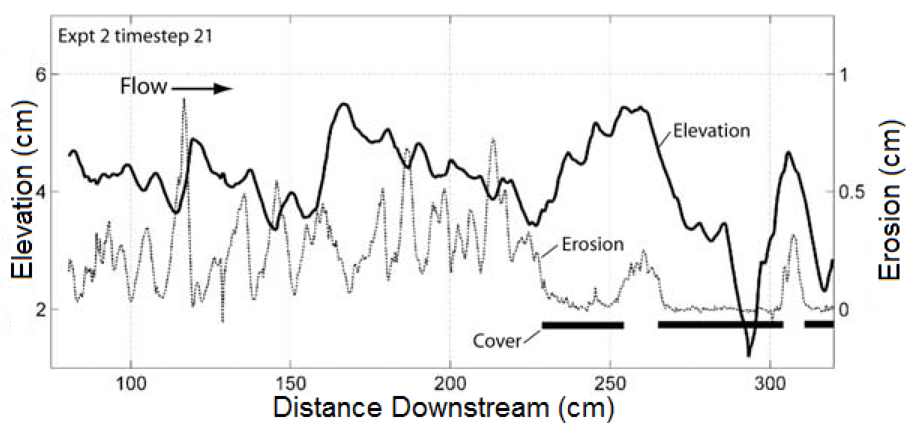

Figure 4.2: A flume experiment by *Johnson and Whipple* [2010] shows that erosion is concentrated on the flow-facing slopes.

Wilson et al. [2013] investigate the processes that form and erode bedrock bedforms shaped much like the bump used in this study. First described by *Richardson and Carling*

[2005], upstream-facing convex surfaces are widespread and are formed with a crest line perpendicular to flow. Based on observations in the field and in flow experiments, *Wilson et al.* [2013] argue that these bedforms are formed and shaped by bedload abrasion. In the absence of flow separation, erosion is concentrated on the upstream face, where most impacts occur. The model presented here matches these observations. However, in the case of flow separation, erosion is dominated by suspended load abrasion, creating potholes on the lee side of bumps within the flow [e.g. *Hancock et al.*, 1998; *Whipple et al.*, 2000; *Wilson et al.*, 2013].

Chapter 5

Conclusions

Simple bed topography can increase erosion rates due to abrasion by bed load by orders of magnitude even if the topography is small and low-angle. This erosion is focused on flow-facing slopes, as seen in in the field [e.g. *Whipple et al.*, 2000; *Wilson et al.*, 2013] and in flume experiments [e.g. *Johnson and Whipple*, 2010]. With simple topography, erosion is maximal with strong flows and small grains, contrary to the findings of *Sklar and Dietrich* [2004], which predicts maximum erosion over flat topography with moderate flows and medium grains. This finding is independent of the angle and size of the topography. It is important, therefore, to consider bed topography when attempting to estimate erosion rates in bedrock streams.

Bibliography

Abbott, J. E., and J. R. D. Francis (1977), Saltation and Suspension Trajectories of Solid Grains in a Water Stream, *Royal Society of London Philosophical Transactions Series A*, *284*, 225–254, doi: 10.1098/rsta.1977.0009.

Allen, J. (1971), Transverse erosional marks of mud and rock: their physical basis and geological significance, *Sedimentary Geology*, *5*, 167–385, doi:10.1016/0037-0738(71)90001-7.

Anderson, R. S. (1986), Erosion profiles due to particles entrained by wind: Application of an eolian sediment-transport model, *Geological Society of America Bulletin*, *97*, 1270, doi:10.1130/0016-7606(1986)97¡1270:EPDTPE¿2.0.CO;2.

Anderson, R. S. (1994), Evolution of the Santa Cruz Mountains, California through tectonic growth and geomorphic decay, *Journal of Geophysical Research*, *99*, 20,161, doi:10.1029/94JB00713.

Anderson, R. S., and P. K. Haff (1988), Simulation of eolian saltation, *Science*, *241*(4867), 820–823, doi: 10.1126/science.241.4867.820.

Barnes, H. L. (1956), Cavitation as a Geological Agent, *American Journal of Science*, *254*, 493 – 505, doi: 10.2475/ajs.254.8.493.

Bitter, J. (1963), A study of erosion phenomena part i, *Wear*, *6*(1), 5 – 21, doi:10.1016/0043-1648(63)90003-6.

Chatanantavet, P., and G. Parker (2009), Physically based modeling of bedrock incision by abrasion, plucking, and macroabrasion, *Journal of Geophysical Research (Earth Surface)*, *114*, F04018, doi: 10.1029/2008JF001044.

Chaudhry, M. H. (1993), *Open-Channel Flow*, 483 pp., Prentice-Hall; Englwood Cliffs, New Jersey.

Chow, V. T. (1959), *Open-Channel Hydraulics*, 680 pp., McGraw-Hill; New York, New York.

D'Errico, J. (2009), SLM - Shape Language Modeling, *MATLAB Central File Exchange*, (updated 2012), <http://www.mathworks.com/matlabcentral/fileexchange/24,443–slm–shape–language–modeling>.

Einstein, H. A. (1950), The bed-load function for sediment transportation in open channel flows, *U. S. Dept. of Agriculture Tech. Bull.*, *1026*, 1–71.

Engel, P. A. (1976), *Impact wear of materials*, 339 pp., Elsevier Scientific Pub. Co.; New York, New York.

Fernandez-Luque, R., and R. van Beek (1976), Erosion and transport of bed-load sediment, *Journal of Hydraulic Research*, *14*, 127–144.

Finnie, I. (1960), Erosion of surfaces by solid particles, *Wear*, *3*(2), 87 – 103, doi:10.1016/0043-1648(60)90055-7.

Goode, J. R., and E. Wohl (2010), Substrate controls on the longitudinal profile of bedrock channels: Implications for reach-scale roughness, *Journal of Geophysical Research: Earth Surface*, *115*(F3), F03018, doi:10.1029/2008JF001188.

Hancock, G. S., and R. S. Anderson (2002), Numerical modeling of fluvial strath-terrace formation in response to oscillating climate, *Geological Society of America Bulletin*, *114*(9), 1131–1142, doi:10.1130/0016-7606(2002)114¡1131:NMOFST¿2.0.CO;2.

Hancock, G. S., R. S. Anderson, and K. X. Whipple (1998), Beyond power: Bedrock river incision process and form, *American Geophysical Union Geophysical Monograph Series*, *107*, 35–60, doi:10.1029/GM107p0035.

Hancock, G. S., E. E. Small, and C. Wobus (2011), Modeling the effects of weathering on bedrock-floored channel geometry, *Journal of Geophysical Research*, *116*, F03018, doi:10.1029/2010JF001908.

Howard, A. D., W. E. Dietrich, and M. A. Seidl (1994), Modeling fluvial erosion on regional to continental scales, *Journal of Geophysical Research*, *99*, 13,971, doi:10.1029/94JB00744.

Hu, C., and Y. Hui (1996a), Bed-load transport. i: Mechanical characteristics, *Journal of Hydraulic Engineering*, *122*(5), 245–254, doi:10.1061/(ASCE)0733-9429(1996)122:5(245).

Hu, C., and Y. Hui (1996b), Bed-load transport. ii: Stochastic characteristics, *Journal of Hydraulic Engineering*, *122*(5), 255–261, doi:10.1061/(ASCE)0733-9429(1996)122:5(255).

Johnson, J. P., and K. X. Whipple (2007), Feedbacks between erosion and sediment transport in experimental bedrock channels, *Earth Surface Processes and Landforms*, *32*(7), 1048–1062, doi:10.1002/esp.1471.

Johnson, J. P. L., and K. X. Whipple (2010), Evaluating the controls of shear stress, sediment supply, alluvial cover, and channel morphology on experimental bedrock incision rate, *Journal of Geophysical Research (Earth Surface)*, *115*, F02018, doi:10.1029/2009JF001335.

Lamb, M. P., W. E. Dietrich, and L. S. Sklar (2008), A model for fluvial bedrock incision by impacting suspended and bed load sediment, *Journal of Geophysical Research*, *113*, F03025, doi:10.1029/2007JF000915.

Lee, H.-Y., and I.-S. Hsu (1994), Investigation of saltating particle motions, *Journal of Hydraulic Engineering*, *120*(7), 831–845, doi:10.1061/(ASCE)0733-9429(1994)120:7(831).

Montgomery, D. R., and J. M. Buffington (1997), Channel-reach morphology in mountain drainage basins, *Geological Society of America Bulletin*, *109*(5), 596–611, doi:10.1130/0016-7606(1997)109<0596:CRMIMD>2.3.CO;2.

Nasrollahi, A., S. A. A. Salehi Neyshabouri, G. Ahmadi, and M. M. Namin (2008), Numerical simulation of particle saltation process, *Particulate Science and Technology*, *26*(6), 529–550, doi: 10.1080/02726350802498723.

Nezu, I., and H. Nakagawa (1993), *Turbulence in Open-Channel Flows*, 281 pp., Balkema; Rotterdam, The Netherlands.

Niño, Y., M. García, and L. Ayala (1994), Gravel saltation: 1. experiments, *Water Resources Research*, *30*(6), 1907–1914, doi:10.1029/94WR00533.

Richardson, K., and P. Carling (2005), *Typology of Sculpted Forms in Open Bedrock Channels*, Special Paper 392, 108 pp., Geological Society of America, Boulder, CO.

Rubinow, S. I., and J. B. Keller (1961), The transverse force on a spinning sphere moving in a viscous fluid, *Journal of Fluid Mechanics*, *11*, 447–459, doi:10.1017/S0022112061000640.

Sekine, M., and H. Kikkawa (1992), Mechanics of saltating grains. ii, *Journal of Hydraulic Engineering*, *118*(4), 536–558, doi:10.1061/(ASCE)0733-9429(1992)118:4(536).

Sklar, L. S. (2003), The influence of grain size, sediment supply, and rock strength on rates of river incision into bedrock, Ph.D. thesis, Univ. of California, Berkeley.

Sklar, L. S., and W. E. Dietrich (2001), Sediment and rock strength controls on river incision into bedrock, *Geology*, *29*, 1087, doi:10.1130/0091-7613(2001)029<1087:SARSCO>2.0.CO;2.

Sklar, L. S., and W. E. Dietrich (2004), A mechanistic model for river incision into bedrock by saltating bed load, *Water Resources Research*, *40*, W06301, doi:10.1029/2003WR002496.

Stock, J. D., and D. R. Montgomery (1999), Geologic constraints on bedrock river incision using the stream power law, *Journal of Geophysical Research*, *104*, 4983–4993, doi:10.1029/98JB02139.

Tucker, G. E., and R. L. Slingerland (1994), Erosional dynamics, flexural isostasy, and long-lived escarpments: A numerical modeling study, *Journal of Geophysical Research*, *99*, 12,229, doi:10.1029/94JB00320.

Turowski, J. M., D. Lague, and N. Hovius (2007), Cover effect in bedrock abrasion: A new derivation and its implications for the modeling of bedrock channel morphology, *Journal of Geophysical Research: Earth Surface*, *112*(F4), F04006, doi:10.1029/2006JF000697.

Turowski, J. M., N. Hovius, H. Meng-Long, D. Lague, and C. Men-Chiang (2008), Distribution of erosion across bedrock channels, *Earth Surface Processes and Landforms*, *33*, 353–363, doi:10.1002/esp.1559.

Whipple, K. X. (2004), Bedrock Rivers and the Geomorphology of Active Orogens, *Annual Review of Earth and Planetary Sciences*, *32*, 151–185, doi:10.1146/annurev.earth.32.101802.120356.

Whipple, K. X., and G. E. Tucker (1999), Dynamics of the stream-power river incision model: Implications for height limits of mountain ranges, landscape response timescales, and research needs, *Journal of Geophysical Research*, *104*, 17,661–17,674, doi:10.1029/1999JB900120.

Whipple, K. X., and G. E. Tucker (2002), Implications of sediment-flux-dependent river incision models for landscape evolution, *Journal of Geophysical Research*, *107*, 2039, doi:10.1029/2000JB000044.

Whipple, K. X., G. S. Hancock, and R. S. Anderson (2000), River incision into bedrock: Mechanics and relative efficacy of plucking, abrasion, and cavitation, *Geological Society of America Bulletin*, *112*(3), 490–503, doi:10.1130/0016-7606(2000)112<490:RIIBMA>2.0.CO;2.

Wiberg, P. L., and J. D. Smith (1985), A theoretical model for saltating grains in water, *Journal of Geophysical Research*, *90*, 7341–7354, doi:10.1029/JC090iC04p07341.

Wilson, A., N. Hovius, and J. M. Turowski (2013), Upstream-facing convex surfaces: Bedrock bedforms produced by fluvial bedload abrasion, *Geomorphology*, *180*, 187–204, doi:10.1016/j.geomorph.2012.10.010.

Wobus, C. W., G. E. Tucker, and R. S. Anderson (2006), Self-formed bedrock channels, *Geophysical Research Letters*, *33*(18), L18408, doi:10.1029/2006GL027182.

Wohl, E. E. (1993), Bedrock Channel Incision along Piccaninny Creek, Australia, *Journal of Geology*, *101*, 749–761, doi:10.1086/648272.

Wohl, E. E., and H. Ikeda (1997), Experimental simulation of channel incision into a cohesive substrate at varying gradients, *Geology*, *25*, 295, doi:10.1130/0091-7613(1997)025<0295:ESOCII>2.3.CO;2.

Wohl, E. E., and H. Ikeda (1998), Patterns of Bedrock Channel Erosion on the Boso Peninsula, Japan, *Journal of Geology*, *106*, 331–346, doi:10.1086/516026.

Wohl, E. E., and D. M. Merritt (2001), Bedrock channel morphology, *Geological Society of America Bulletin*, *113*(9), 1205–1212, doi:10.1130/0016-7606(2001)113<1205:BCM>2.0.CO;2.

Appendix A

List of Symbols

A_{tot}	total area traversed
A_u	area traversed over the upslope
A_d	area traversed over the downslope
D_s	sediment grain diameter
E	erosion rate
E_u	erosion rate on flow-facing slopes
E_d	erosion rate on slopes facing downflow
E_f	erosion rate along flat topography
F_e	exposed fraction of the bed
Fr	Froude number
H_s	saltation hop height
H_w	flow depth
I_r	impact rate per unit area
I_{ru}	impact rate per width along upslope
I_{rd}	impact rate per width along downslope
K_p	kinetic energy transferred to bed
$\overline{L_s}$	average saltation hop length
L_s	saltation hop length of specific hop
$\overline{L_{sd}}$	average horizontal length of saltation hop descent
L_{sd}	horizontal length of specific saltation hop descent
L_{su}	horizontal length of saltation hop ascent
Q_s	sediment mass flux
Q_w	channel discharge
R_b	nondimensional buoyant density of sediment
S_i	impact speed
V_i	volume eroded per impact
W	channel width
Y	Young's Modulus of the bed
g	gravitational acceleration
h_c	critical flow depth
i_u	impact rate (per particle) on the upslope

i_d	impact rate (per particle) on the downslope
k_v	dimensionless coefficient $= 10^6$
l	total horizontal length of topography
l_{up}	horizontal length of flow-facing slope
m	mass flux per width per particle
n	number of impacts
n_u	number of impacts on (flow-facing) upslope
n_d	number of impacts on downslope
n_m	Manning's roughness of the channel
q_s	sediment mass flux per unit width
q_t	sediment transport capacity per unit width
t_{tot}	total time of simulation
t_u	time grain spends above the upslope
t_d	time grain spends above the downslope
u	downstream flow velocity
u_{sf}	horizontal component of sediment velocity upon return to takeoff height
u_{si}	horizontal component of sediment impact velocity
$\overline{u_s}$	average horizontal velocity of saltating sediment grain through hop
u_{su}	horizontal velocity of saltating sediment grain along ascent
u_*	friction velocity of the flow
v_n	component of sediment impact velocity normal to the bed
w_{si}	vertical component of sediment impact velocity
w_{sd}	mean sediment particle descent velocity
$\overline{w_{sf}}$	average vertical component of sediment velocity upon return to takeoff height
w_{sf}	vertical component of sediment velocity upon return to takeoff height of specific hop
w'	deviatoric vertical sediment particle velocity associated with turbulence
x	horizontal position of saltating grain
z	vertical position of saltating grain
Φ	channel slope
β	capacity to store energy elastically
ϵ_t	threshold energy required for detachment
ϵ_v	total energy required to erode a unit volume of rock
θ	angle of flow-facing slope
ξ	impact angle (angle between impacting trajectory and topography)
ρ_s	density of sediment grains
ρ_w	density of water
σ_T	tensile yield stress of the bed
τ^*	nondimensional boundary shear stress
τ_b	boundary shear stress
τ_c^*	value of τ^* at threshold of particle motion
τ^*/τ_c^*	transport stage (nondimensional shear stress)
$\tau^*/\tau_c^* - 1$	nondimensional excess shear stress
ψ	saltation takeoff angle